Sofia University "St. Kliment Ohridski"
Faculty of physics
Department of atomic physics

Moment of inertia of ^{98}Sr in an explictly particle number conserving approach

Master thesis
of
Konstantin Georgiev Shegunov
Nuclear and particle physics, №160263

Thesis supervisor:
Asst. Prof. Ludovic Bonneau
Scientific consultants:
Asst. Prof. Hristo Lafchiev
Prof. Emer. Philippe Quentin

Department head:
Assoc. Prof. Georgi Rainovski

9.V.2013
Sofia

Abstract

In the present work a small number of methods used for describing nuclei are covered along with some practical considerations on their use and applicability. These methods are employed to provide theoretical information on some ground state properties of the ^{98}Sr nucleus, which are compared with the experimentally available data. A detailed analysis and a summary is provided for the sensitivity of the nuclear moment of inertia in relation to the amount of pairing correlations. All the aforementioned treatments are performed in the context of the Highly Truncated Diagonalization Approach (HTDA) whence all relevant information is obtained.

Contents

Chapter 1

Introduction

Nuclear physics, despite its short existence, has provided an enormous factual diversity from experiments and numerous models attempting to systematize the behaviour of nuclear matter. Notwithstanding the distinct number of models available, there is not one which can attribute all the known nuclear properties to their respective nuclei over the set of all known isotopes. The nuclear theory is a multifaceted field encompasing two major groups – collective (macroscopic) and microscopic models, and in this work a small number of the latter are considered.

Being a theoretical investigation, the text is focused on some of the more recent models used for analysis of the nuclear strucure. The method selected – the Highly Truncated Diagonalization Approach – is a member of the shell-model family, but it is unique in that manner, as it does not treat the one-body problem, but instead focuses on the more complex question of the nuclear many-body description directly. A number of previous studies were performed establishing it as reliable means of obtaining some valuable insight into the nuclear structure [1–7]. When breaking the particle number symmetry is undesirable and will introduce spuriousness in the physical observables, hence the HFB types of methods are not applicable, then HTDA is exceptionally suitable [3].

Pairing as a nuclear phenomenon was proposed on the basis of several experimentally established facts, which will be discussed in the following chapter. One of the observations made was that pairing seems to strongly favor particles coupling to zero angular momentum. The delta interaction was proposed as a possible *pairing force* and it was an enormous success, as it provided explanation for many of the experimentally observed phenomena [8]. The simple form and good properties make it very good in describing the cases where one has to account for the higher terms in the multipole expansion. Unfortunately, to complete the space one has to impose artificially the lower multipoles as well [4]. On the other hand, a finite range interaction, for all intents and purposes of this text – one of gaussian type, is expected to allow probing of couplings to higher angular momenta in the partial wave expansion without explicitly including any of the quadrupole, octupole, etc. operators. Additionally, the finite

range force lifts the symmetry imposed on the spin-isospin channels, and allows to explore each one individually [4, 9, 10].

Chapter 2

Theoretical models

2.1 Mean field theory

Although ostensibly simplistic, the treatment of the many-body problem by the mean field ansatz has proven to be very successful. Similarly on how electrons are placed and are moving in a central electromagnetic field created by the charge of the nucleus, it is supposed that nucleons inside the nucleus are interacting in the same manner with a central field, even though no such real object exists. The observation that nucleons have a length of the free run of the same magnitude as the size of the nucleus makes possible to accept the notion of independent particles moving in an "averaged" potential and this is strongly supported by the emergence of "magic" numbers similarly to the case with the electrons in the atom. While not real, the mean field is simply a clever way to approximate the numerous interactions in which each nucleon takes part inside the core matter with a single "effective" one. The method substitutes the many-body problem with a one-body problem, thus providing enormous simplification to the equations which need to be solved, while keeping at least part of the correlations existing between the nucleons. Of course, such a scheme does not come free and it has been shown that important physical phenomena can not be explained by the mean field theory alone [8, 11].

Obtaining the "real" mean field is a task which is ill defined by the core asumptions made by the theory itself. Nevertheless, by making the reasonable supposition that the average potential is approximately following the nuclear density, an analitycal formula can be provided for the mean field - the Woods-Saxon potential [12]:

$$V(r) = -V_0 \frac{1}{1 + \exp\left[\frac{1}{a}(r - R)\right]} \tag{2.1}$$

where V_0 is the depth, a the surface thickness of the nucleus and $R = r_0 A^{1/3}$ the nuclear radius ($r_0 = 1.25\,\mathrm{fm}$). It, being proposed on the basis of the aforementioned observation, was shown to give quite acceptable results in the context of the mean field theory. Unfortunately, the

wavefunctions for this potential could not be obtained in a closed form, which is a regrettable failing and makes it inapplicable directly to shell model calculations.

Often in the field of nuclear theory, when treating problems associated with the mean field, a transformation of the Hamiltonian is made, splitting it to a one-body and a many-body (usually a two-body) parts. This is helpful in numerous cases where the mean field is treated by known and established methods, while the residual part is the one of real interest. Furthermore, it is shown that the residual interaction is indeed the one which lifts degeneracies on the energy otherwise unresolved by the *averaged* potential [8]. Starting from a general Hamiltonian, a separation can be made, such that:

$$\hat{H} = \hat{T} + \hat{V} = \underbrace{(\hat{T} + \hat{U})}_{\hat{H}_0} + \underbrace{(\hat{V} - \hat{U})}_{\hat{V}_{\text{res}}} \tag{2.2}$$

where $\hat{U}$ is an arbitrary one-body field, $\hat{H}_0$ is the one-body Hamiltonian and $\hat{V}_{\text{res}}$ is the residual many-body interaction.

2.2 The Hartree-Fock method

The mean field theory simplifies the task of accounting for all nucleon interactions separately by introducing an average potential, but it still does not provide a reasonable method for extracting physical information apart from solving the Schrödinger equation explicitly. This defficiency can be resolved by using the Hartree-Fock method, which provides an approach to finding an approximation for the quantum system wavefunction and the corresponding energy simultaneously from a given two-body interaction.

Ignoring relativistic effects, the Hamiltonian in some complete orthonormal basis of single-particle states can be written as:

$$\hat{H} = \sum_{i,j} \langle i|\hat{T}|j\rangle \hat{a}_i^\dagger \hat{a}_j + \frac{1}{2} \sum_{i,j,k,l} \langle ij|\hat{V}|kl\rangle \hat{a}_i^\dagger \hat{a}_j^\dagger \hat{a}_l \hat{a}_k \tag{2.3}$$

where $\hat{a}_i^\dagger$ and $\hat{a}_i$ are the creation and anihilation operators respectively for some single-particle state i. It is then possible to formally expand a single eigenstate of that Hamiltonian through all states with the same number of nucleons:

$$|\Psi\rangle = \sum_{i_1 \ldots i_A} C_{i_1 \ldots i_A} |i_1 \ldots i_A\rangle \tag{2.4}$$

The states $|i_1 \ldots i_A\rangle$ are called Hartree products and are obtained by simply occupying the

single-particle states over the single-particle vacuum:

$$|i_1 \dots i_A\rangle = \prod_{k=1}^{A} \hat{a}^\dagger_{i_k} |-\rangle \tag{2.5}$$

It is obvious that an expansion like (2.4) is not tractable in general, because of the overwhelming number of possible combinations for the indices $\{i_k\}$. To solve this problem one either has to significantly reduce the number of particles and levels involved, or substitute the wavefunction expansion with a simpler one. In the context of the Hartree-Fock ansatz the latter is employed by imposing the restriction of using a single term in the expansion. While this indeed provides simplification it also removes the possibility of choosing arbitrarily the single-particle wavefunctions, but instead they have to be provided by the method itself [8].

An unfortunate consequence of using a single term in the expansion is that the state $|\Psi\rangle$ is not an exact eigenstate of the Hamiltonian anymore, but an approximation to one. Furthermore, another problem presents itself in the context of particle correlations – they are not included at all, instead the nucleons are independent of one another [8]. To account at least for the Pauli principle it is necessary to introduce a way for the particles to be strongly correlated in respect to their position. This is done straightforwardly by antisymmetrisation of the many-body wavefunction:

$$|\Psi\rangle = \frac{1}{\sqrt{A!}} \sum_P \mathrm{sgn}(P) P |i_1 \dots i_A\rangle \tag{2.6}$$

where P are the permutation matrices of order A, and $\mathrm{sgn}(P)$ are the corresponding permutation signatures.

It was mentioned that because of the enforcement of a specific simple form for the quantum system wavefunction it is required that the method provide a way of deducing the basis of single-particle states. By applying the Ritz variational principle and minimizing the energy functional, it is possible to obtain the single-particle basis of the system iteratively. While it is feasible to apply the Hartree-Fock approach for excited nuclear states, it is most common and most convenient to use it for obtaining the many-body ground state [8, 11].

According to the Ritz variational principle, requiring the energy functional to be minimal:

$$\delta E[\Psi] = 0 \quad \text{where} \quad E[\Psi] = \frac{\langle \Psi | \hat{H} | \Psi \rangle}{\langle \Psi | \Psi \rangle} \tag{2.7}$$

is equivalent to solving the Schrödinger equation:

$$\hat{H}|\Psi\rangle = E|\Psi\rangle \tag{2.8}$$

By varying the wavefunction through single-particle excitations:

$$|\delta\Psi\rangle = \varepsilon \hat{a}^\dagger_m \hat{a}_n |\Psi\rangle \tag{2.9}$$

and substituting back in equations (2.7):

$$\langle \delta\Psi|\hat{H}|\Psi\rangle = \varepsilon^*\langle\Psi|\hat{a}_m^\dagger\hat{a}_n\hat{H}|\Psi\rangle = 0 \tag{2.10}$$

one can obtain the variation equation, by dropping the unimportant coefficient ε:

$$\langle\Psi|\hat{a}_m^\dagger\hat{a}_n\hat{H}|\Psi\rangle = 0 \tag{2.11}$$

which is then reduced to the requirement that the Hartree-Fock Hamiltonian is diagonal:

$$\langle i|\hat{h}_{\mathrm{HF}}|j\rangle = \langle i|\hat{T}|j\rangle + \sum_{k=1}^{A}\langle ik|\hat{V}|jk\rangle = \varepsilon_i\delta_{ij} \tag{2.12}$$

Equation (2.12) provides the criterion by which to obtain the canonical basis and supplies the single-particle energies ε_i, each one of which is interpreted as the separation energy for a given nucleon. The total energy is then given as [8, 11]:

$$E_{\mathrm{HF}} = \sum_{i=1}^{A}\varepsilon_i - \frac{1}{2}\sum_{ij=1}^{A}\langle ij|\hat{V}|\widetilde{ij}\rangle \tag{2.13}$$

2.3 The BCS model

As it was discussed, the Hartree-Fock model provides a consistent approach to finding an approximate many-body wavefunction for a given two-body interaction. Unfortunately, it fails to incorporate correlations beyond the mean-field, an important case of this shortcoming being the pairing of nucleons. Introducing pairing was historically guided by several established experimental facts [8, 13]:

- The ground state of even-even nuclei always has zero angular momentum.
- Binding energy is larger for even-even compared to odd nuclei.
- An energy gap of 1 MeV to 2 MeV is apparent between the ground state and the first single particle excitation in even-even nuclei.

These observations led to the conclusion that coupling to zero angular momentum is strongly favored and the residual interaction must lift the angular momenta's degeneracy. The BCS model provides a framework to treat the pairing correlations in nuclei by introducing pairs of degenerate and mutually time-reversal conjugate states. The theory was adapted from the solid-state physics where it was developed to account for superconductivity and there the pairs are of coupled-momentum eigenstates, while for the nucleus the "good" quantum number is the angular momentum projection onto the the intrinsic axis [11].

Given two eigenstates of the $\hat{J}_z$ operator:

$$\begin{aligned} \hat{J}_z|k\rangle &= \Omega_k|k\rangle \\ \hat{J}_z|\overline{k}\rangle &= \Omega_{\overline{k}}|k\rangle \end{aligned} \tag{2.14}$$

and acknowledging $\left\{\hat{J}_z, \hat{\mathcal{T}}\right\} = 0$, where $\hat{\mathcal{T}}$ is the time reversal operator, it straightforwardly follows that:

$$\Omega_{\overline{k}} = -\Omega_k \tag{2.15}$$

Equations (2.14) and (2.15) show that $|k\rangle$ and $|\overline{k}\rangle$ are states that form a time reversal conjugate pair:

$$\begin{aligned} \hat{\mathcal{T}}|k\rangle &= |\overline{k}\rangle \\ \hat{\mathcal{T}}|\overline{k}\rangle &= -|k\rangle \end{aligned} \tag{2.16}$$

The cornerstone of BCS theory is the Bogoliubov-Valatin transformation by which the quasiparticle creation and anihilation operators ($\hat{b}_k^\dagger$ and $\hat{b}_k$) are introduced through linear combinations of their fermionic counterparts [11]:

$$\hat{b}_k^\dagger = u_k\hat{a}_k^\dagger - v_k\hat{a}_{\overline{k}} \qquad \hat{b}_k = u_k\hat{a}_k - v_k\hat{a}_{\overline{k}}^\dagger \tag{2.17}$$

$$\hat{b}_{\overline{k}}^\dagger = u_k\hat{a}_{\overline{k}}^\dagger + v_k\hat{a}_k \qquad \hat{b}_{\overline{k}} = u_k\hat{a}_{\overline{k}} + v_k\hat{a}_k^\dagger \tag{2.18}$$

where u_k and v_k are real numbers and take values between 0 and 1.

The BCS ground state can be expressed from the single particle vacuum with the help of the coefficients u_i and v_i:

$$|\mathrm{BCS}\rangle = \prod_{k>0}\left(u_k + v_k\hat{a}_k^\dagger\hat{a}_{\overline{k}}^\dagger\right)|-\rangle \tag{2.19}$$

whence:

$$\begin{aligned} \hat{b}_k|\mathrm{BCS}\rangle &= 0 \\ \hat{b}_{\overline{k}}|\mathrm{BCS}\rangle &= 0 \end{aligned} \tag{2.20}$$

In this case the probability of a pair $\left(k, \overline{k}\right)$ being occupied is given by $|v_k|^2$ and the probability that it remains empty is measured by $|u_k|^2$. The form of the ground state allows to treat $|\mathrm{BCS}\rangle$ as a quasi-vacuum in respect to the quasiparticle ladder operators (2.20). As with most cases, it is required for the ground state wavefunction to be normalized:

$$\langle\mathrm{BCS}|\mathrm{BCS}\rangle = \langle-|\prod_{k_1>0}\left(u_{k_1} + v_{k_1}\hat{a}_{\overline{k}_1}\hat{a}_{k_1}\right)\prod_{k_2>0}\left(u_{k_2} + v_{k_2}\hat{a}_{\overline{k}_2}^\dagger\hat{a}_{k_2}^\dagger\right)|-\rangle \tag{2.21}$$

The terms within the parenthesis all commute for different k_1 and k_2, thus the only relevant product that needs to be considered is when $k_1 = k_2 = k$. The expression then reduces to:

$$\langle \mathrm{BCS}|\mathrm{BCS}\rangle = \prod_{k>0} \left(u_k^2 + v_k^2\right) \tag{2.22}$$

Whence the normalization condition could be extracted:

$$u_k^2 + v_k^2 = 1 \tag{2.23}$$

From the mixing of creation and annihilation operators it can be deduced that the particle number is not preserved, and indeed, writing the expectation value for the particle number operator shows that explicitly:

$$N = \langle \mathrm{BCS}|\hat{N}|\mathrm{BCS}\rangle = \langle \mathrm{BCS}| \sum_{k>0} \left(\hat{a}_k^\dagger \hat{a}_k + \hat{a}_{\overline{k}}^\dagger \hat{a}_{\overline{k}}\right) |\mathrm{BCS}\rangle = 2\sum_{k>0} v_k^2 \tag{2.24}$$

While in solid state physics the particle number violation is of no real consequence, because $N \simeq 10^{23}$, this is not the case in nuclei, where the particle number symmetry should be strictly observed. Otherwise serious errors may occur in treating the nuclear phenomena [8]. Starting from the Hartree-Fock many-body Hamiltonian (2.3) and rewriting it to use the potential's antisymmetrized matrix element, it becomes:

$$\hat{H} = \sum_{i,j} \langle i|\hat{T}|j\rangle \hat{a}_i^\dagger \hat{a}_j + \frac{1}{4} \sum_{i,j,k,l} \langle ij|\hat{V}|\widetilde{kl}\rangle \hat{a}_i^\dagger \hat{a}_j^\dagger \hat{a}_l \hat{a}_k \tag{2.25}$$

To enforce the conservation of the particle number a term is added to the Hamiltonian:

$$\hat{H}_{\mathrm{var}} = \hat{H} - \lambda \hat{N} \tag{2.26}$$

The introduced *Lagrange multiplier* λ is called either *chemical potential* or *Fermi energy*, because it represents how the total energy changes for a change of the number of particles [11]. The condition which fixes the Fermi energy is (2.24).

Performing the variation:

$$\delta \langle \mathrm{BCS}|\hat{H}_{\mathrm{var}}|\mathrm{BCS}\rangle = 0 \tag{2.27}$$

yields:

$$\widetilde{\varepsilon}_k = \frac{1}{2}\left[\langle k|\hat{T}|k\rangle + \langle \overline{k}|\hat{T}|\overline{k}\rangle + \sum_{m\neq 0} v_m^2 \left(\langle km|\hat{V}|\widetilde{km}\rangle + \langle \overline{k}m|\hat{V}|\widetilde{\overline{k}m}\rangle\right)\right] - \lambda \tag{2.28}$$

$$\Delta_k = \sum_{m>0} u_m v_m \langle k\overline{k}|\hat{V}|\widetilde{m\overline{m}}\rangle \tag{2.29}$$

$$v_k^2 = \frac{1}{2}\left(1 - \frac{\widetilde{\varepsilon}_k}{\sqrt{\widetilde{\varepsilon}_k^2 + \Delta_k^2}}\right) \qquad u_k^2 = \frac{1}{2}\left(1 + \frac{\widetilde{\varepsilon}_k}{\sqrt{\widetilde{\varepsilon}_k^2 + \Delta_k^2}}\right) \tag{2.30}$$

These equations together with the particle number formula (2.24) form the BCS equations and allow the calculation of the coefficients v_k and u_k. As can be seen, they are nonlinear and have to be solved iteratively [11].

2.4 The Highly Truncated Diagonalization Approximation

In the Hartree-Fock approach an assumption is made that the nucleus' wavefunction can be described by a single Slater determinant from the infinite expansion. Unfortunately, the method does not include corelations beyond the mean field. Its derived approaches HF+BCS and HFB do improve on that deficiency, but prove to be somewhat inconvenient as results need to be projected so particle number is conserved. The HTDA method was conceived to provide a shell model alike treatment for the many-body problem, thus not breaking the particle number symmetry [1, 3].

2.4.1 Formalism

To derive the HTDA ansatz one starts from a Hamiltonian with a two-body interaction $\hat{V}$:

$$\hat{H} = \hat{T} + \hat{V} \tag{2.31}$$

which is then separated to a one-body part and a two-body part with the help of $\hat{U}$ – a one-body potential [14]:

$$\hat{H} = \underbrace{(\hat{T} + \hat{U})}_{\hat{H}_0} + \underbrace{(\hat{V} - \hat{U})}_{\hat{V}_{\text{res}}} \tag{2.32}$$

Here $\hat{H}_0$ is the one-body Hamiltonian, having a ground state $|\Phi_0\rangle$ represented by a single Slater determinant and $\hat{V}_{\text{res}}$ is the remaining two-body *residual* interaction. HTDA consists of building a many-body basis on top of the state $|\Phi_0\rangle$ and minimizing the Hamiltonian expectation value of Ψ – the nucleus wavefunction, expanded in that basis [1].

As already mentioned, for the reference Slater determinant a solution of a HF+BCS procedure is considered. Then the basis could be represented by:

$$|\Phi_m^{(n)}\rangle = \prod_{i,j}^{n} \hat{a}_{m_i}^{\dagger} \hat{a}_{m_j} |\Phi_0\rangle \tag{2.33}$$

The different configurations are represented by Slater determinants with excitations of the type n-particles-n-holes (npnh) over the reference state.

The nucleus wavefunction expanded in this basis is writen as:

$$|\Psi\rangle = \chi_0|\Phi_0\rangle + \chi_i^{(1)}|\Phi_i^{(1)}\rangle + \chi_i^{(2)}|\Phi_i^{(2)}\rangle + \chi_i^{(3)}|\Phi_i^{(3)}\rangle + \dots \tag{2.34}$$

The amplitudes χ_i are obtained by diagonalization of the Hamiltonian in the many-body basis and furthermore are subject to the normalization condition:

$$\sum_i |\chi_i|^2 = 1 \tag{2.35}$$

Additionally, only real values for χ_i are used, because the HTDA wavefunctions are even, or could be made even, under time reversal [6].

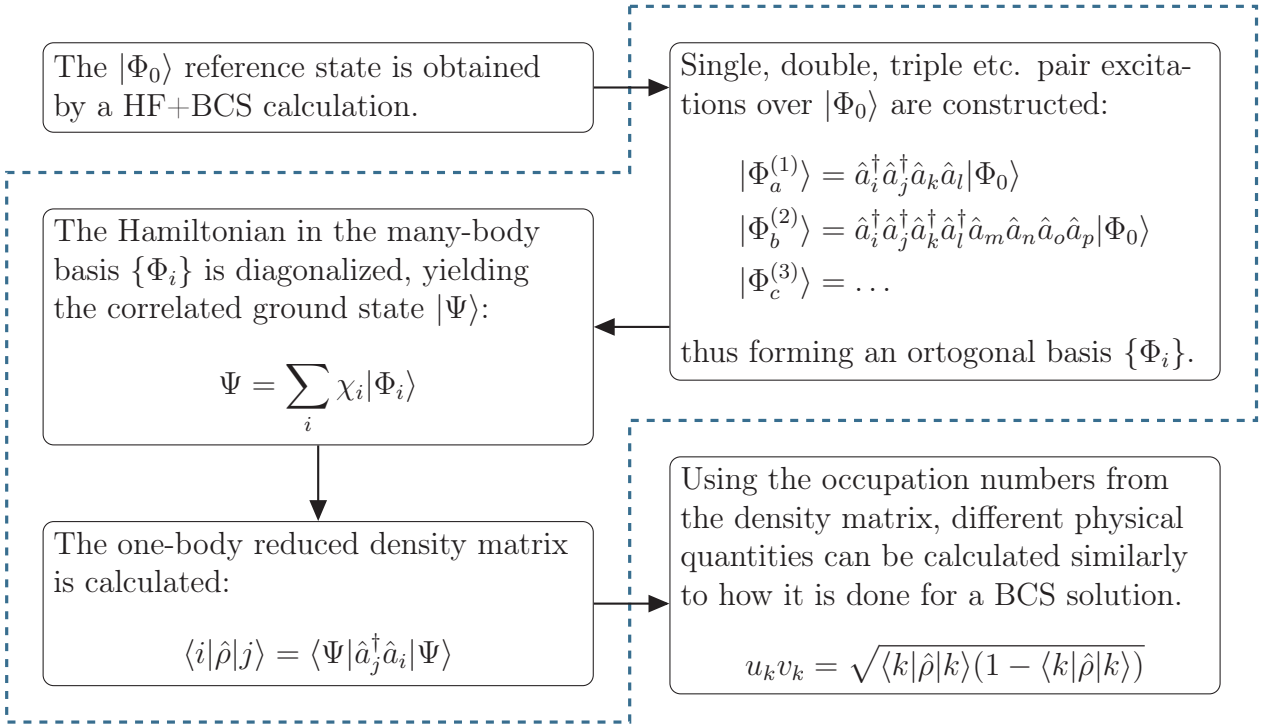

Figure 2.1: Main steps involved in obtaining results with HTDA.

The basis of single particle statesm used for the construction of the Slater determinants $|\Phi_n\rangle$, is obtained from the Hartree-Fock calculation. To describe the exact solution one has to consider an infinite set of single particle states on the one hand, and on the other an infinite number of particle-hole excitations have to be included in the HTDA wavefunction's expansion. This is obviously impossible and some simplifications have to be employed as to make the problem tractable.

Firstly, not all possible excitations are taken, but only a limited number around the Fermi level. Additionally, a smoothing factor is used to reduce stridency in the physical observables, which might occur because of the abrupt changes in single particle energy. Secondly, a truncation is enforced on the number of pair-hole excitations. It is expected that the expansion (2.34) will

converge quickly enough, so excluding part of the terms would not cause much spuriousness to the HTDA wavefunction [1].

The state (2.34) corresponds to an admixture of different n-particle configurations, thus it is by construction an eigenstate of the proton number and neutron number operators.

$$\hat{Z}|\Psi\rangle = Z|\Psi\rangle \qquad \hat{N}|\Psi\rangle = N|\Psi\rangle \tag{2.36}$$

The end solution of the method can be characterized by two principal values – the degree of correlation and the correlation energy. The degree of correlation is most simply assessed by the depopulation of the quasi-vacuum state $|\Phi_0\rangle$:

$$D = 1 - \chi_0^2 \tag{2.37}$$

while the correlation energy is straightforwardly defined as [6]:

$$E_{\text{corr}} = \langle\Psi|\hat{H}|\Psi\rangle - \langle\Phi_0|\hat{H}|\Phi_0\rangle \tag{2.38}$$

2.4.2 The Gogny force's matrix element

Since the many-body matrix element is not and could not be made available in closed form, it is obtained through Wick's theorem, as it is usually done [15]:

$$\begin{aligned}
\hat{b}_{\alpha_1}\hat{b}_{\alpha_2}\hat{b}_{\alpha_3}\hat{b}_{\alpha_4}\hat{b}_{\alpha_5}\ldots\hat{b}_{\alpha_k} = \quad & :\hat{b}_{\alpha_1}\hat{b}_{\alpha_2}\hat{b}_{\alpha_3}\hat{b}_{\alpha_4}\hat{b}_{\alpha_5}\ldots\hat{b}_{\alpha_k}: \\
& + \sum_{\text{single}} \; :\underbrace{\hat{b}_{\alpha_1}\hat{b}_{\alpha_2}}\hat{b}_{\alpha_3}\hat{b}_{\alpha_4}\hat{b}_{\alpha_5}\ldots\hat{b}_{\alpha_k}: \\
& + \sum_{\text{double}} \; :\underbrace{\hat{b}_{\alpha_1}\hat{b}_{\alpha_2}\hat{b}_{\alpha_3}\hat{b}_{\alpha_4}}\hat{b}_{\alpha_5}\ldots\hat{b}_{\alpha_k}: \\
& + \sum_{\text{triple}} \; :\underbrace{\hat{b}_{\alpha_1}\hat{b}_{\alpha_2}\hat{b}_{\alpha_3}\hat{b}_{\alpha_4}\hat{b}_{\alpha_5}\ldots\hat{b}_{\alpha_k}}: \\
& + \sum_{\ldots} \; : \quad \ldots \quad :
\end{aligned} \tag{2.39}$$

where $\hat{b}_{\alpha_k}$ is either a single particle fermionic creation or anihilation operator, and the summation is over all single, double, triple, etc. contractions' normal products. That particular expansion requires the values of at least some matrix elements in the Hartree-Fock basis, but the number of terms is not that great, because the only nonzero contractions are of the type shown (δ_{ij} is the Kronecker symbol):

$$\underbrace{\hat{a}_i\hat{a}_j^\dagger} = \delta_{ij} \tag{2.40}$$

Using a typical representation of the Gogny force's central term [16]:

$$\begin{aligned}\hat{V}_{\text{Gogny}} &= \sum_{S,T,\chi} \left[W_\chi + (-1)^{S+1} B_\chi - (-1)^{T+1} H_\chi - (-1)^{S+T} M_\chi\right] \hat{\mathbb{P}}^S \hat{\mathbb{P}}^T \hat{V}^{(r,\sigma,\tau)} \\ &= \sum_{S,T,\chi} V_\chi(S,T) \hat{\mathbb{P}}^S \hat{\mathbb{P}}^T \hat{V}^{(r,\sigma,\tau)}\end{aligned} \tag{2.41}$$

where $\hat{\mathbb{P}}^S$ and $\hat{\mathbb{P}}^T$ are the spin and isospin projection operators respectively, the matrix element in the Hartree-Fock basis is given by (see appendix C):

$$\langle ij|\hat{V}_{\text{Gogny}}|kl\rangle\Big|_{\text{HF}} = \sum_{S,T,\chi} \sum_{n,o,p,q} c_{in} c_{jo} c_{kp} c_{lq} V_\chi(S,T) G(S,T) \langle no|\hat{V}^{(r)}|pq\rangle\Big|_{\text{HO}} \tag{2.42}$$

where c_{ij} are the known cylindrical harmonic oscillator basis expansion coefficients, $G(S,T)$ is a rational factor induced from the spin-isospin projections and $V_\chi(S,T)$ are the cooresponding magnitudes. The explicit closed form of the spatial component of the matrix element is given in [17]. Evidently, it does not depend on S and T and by manipulating the values of $V_\chi(S,T)$ different channels could be selected and their influence explored.

Chapter 3

Numerical methods

3.1 Calculation setup

For the calculation of the various physical quantities a code developed previously by Julien Le Bloas in Fortran 95 was used. It included the whole procedure needed to obtain results with the exception of incorporation of a Gogny residual interaction evaluated with the *Direct calculaton* method. To proceed with the current work a number of modules and procedures were written, so the aforementioned interaction is included into the computer program. Additionally, an external C++ code was written and incorporated to provide the necessary subroutines for dealing with the hash table storage (see appendix A).

Several parameters affect the values obtained, which are differently important for the current work. While deformation parameters for the harmonic oscillator basis are of little consequence, since the dependence of the moment of inertia of the ground state structure is explored, and all the calculations are done usning the same input, the main quantum number N_0 is of utmost importance as it should be large enough for the HO basis to be able to accomodate the expansions used.

As it was already mentioned, the HTDA approach incorporates an inherent freedom to choose the interaction to be different from the one used in solving the mean-field problem. In particular, there are no constraints put on the way the reference Slater determinant is obtained. In this study for the initial step of determining the particle-hole quasi-vacuum $|\Phi_0\rangle$ a Skyrme force (SIII parametrization) was used [18], while the Gogny force's central term was utilised as a residual interaction for the construction of the HTDA Hamiltonian. The initial mean field potential was chosen to be of the Woods-Saxon type and the calculations were performed with $N_0 = 8$, while preserving the parity symmetry.

The data is obtained by varying the renormalization factors for the Gogny force, thus giving a multidimensional set of values for the different physical quantities. These perturbations in

the factors were separately programmed into the existing code and the output data was further processed by command line bash scripts written for that purpose alone.

3.2 Numerical evaluation

The two-body matrix elements' evaluation was done using Gaussian quadratures of appropriate type, for which purpose an additional module in Fortran was developed providing the special functions required. The values were compared to already available figures obtained by Moshinsky expansion and it was shown that the direct calculation provides similar and consistent results.

3.2.1 Moshinsky expansion

As it is shown in [19] the matrix element can be calculated using the Moshinsky transformation between states with coordinates r_1 and r_2, and states with coordinates r and R such as:

$$r = \frac{r_1 - r_2}{\sqrt{2}} \qquad R = \frac{r_1 + r_2}{\sqrt{2}} \tag{3.1}$$

Aplying the aforementioned transformation, the explicit expression for the matrix element could be obtained (keeping the original notation):

$$\langle 12|\frac{e^{-\frac{r^2}{\sigma^2}}}{\sigma^3}|34\rangle = \mathring{c}_0 \left[\sum_n f^n \sum_p C(n,n',p)A(p)\left(\frac{1}{\sqrt{1+c_z^2\sigma^2}}\right)^{p+1}\right]\left(\sum_{a,b} g^{a,b} W^{c_\perp \sigma}_{(a,b,a',b')}\right) \tag{3.2}$$

where the various coefficients and definitions are found in [19] exactly as written here.

3.2.2 Direct calculation

Alternatively to the use of the Moshinsky expansion, the matrix element could be evaluated directly, as it is suggested in [17] and adapted as shown in appendix B. The closed form obtained there is of the type:

$$\langle ij|\hat{V}^{(r)}|kl\rangle = N_\omega \underbrace{\int_{-\infty}^{\infty}\int_{-\infty}^{\infty} \omega_\xi(\xi_1,\xi_2)e^{-\xi_1^2}e^{-\xi_2^2}d\xi_1 d\xi_2}_{V_\xi} \underbrace{\int_0^\infty\int_0^\infty \omega_\eta(\eta_1,\eta_2)\eta_1^{\Lambda_{ik}}\eta_2^{\Lambda_{jl}}e^{-\eta_1}e^{-\eta_2}d\eta_1 d\eta_2}_{V_\eta} \tag{3.3}$$

where N_ω is simply a normalization coefficient It is clear that the actual evaluation should be done separately for the axial and radial parts, the hope initialy being to obtain faster method

for the otherwise quite computationally heavy process. Acquiring the figures for both integrals was done using a Gauss-Hermite quadrature for V_ξ and the Gauss-Laguerre quadrature rule for V_η, as shown in detail in appendix B.

3.3 Speed and accuracy

3.3.1 Matrix elements in the harmonic oscillator basis

The harmonic oscillator basis matrix elements match to a high degree for both methods – *Moshinsky expansion* and *Direct calculation*. The aquired deviation:

$$\Delta \equiv \langle ij|\hat{V}|kl\rangle\Big|_{\text{Direct}} - \langle ij|\hat{V}|kl\rangle\Big|_{\text{Moshinsky}} \tag{3.4}$$

is less than 10^{-6} for a wide range of values, examples of which can be seen in table 3.1.

n_z				n_r				Λ				$\langle ij\|\hat{V}\|kl\rangle$		
i	j	k	l	i	j	k	l	i	j	k	l	Moshinsky	Direct	Δ
1	1	1	1	0	0	0	0	1	−1	1	−1	−157.946 883 90	−157.946 879 80	4.1×10^{-6}
1	1	0	0	0	0	0	0	1	−1	0	0	76.694 142 72	76.694 140 85	-1.9×10^{-6}
1	1	0	4	0	0	0	0	1	−1	0	0	−37.433 628 89	−37.433 627 87	1.0×10^{-6}
1	1	0	0	0	0	0	1	1	−1	0	0	−13.984 855 82	−13.984 855 48	3.4×10^{-7}
1	1	0	4	0	0	1	0	1	−1	0	0	6.825 865 50	6.825 865 31	-1.9×10^{-7}
0	0	0	0	0	0	0	0	0	0	0	0	−442.128 465 98	−442.128 456 66	9.3×10^{-6}

Table 3.1: Comparison between matrix elements in the harmonic oscillator basis calculated using the direct evaluation method and the Moshinsky expansion formula.

3.3.2 Matrix elements in the Hartree-Fock basis

As expected, the small variations in the matrix elements magnitudes for the harmonic oscillator basis are somewhat more pronounced in the Hartree-Fock basis due to the expansion coefficients and subsequent summation. Additionally, a few truncations made in the *Moshinsky expansion* implementation to accelerate the calculation by discarding some small contributions were implicated for the relatively large differences observed in table 3.2. Nonetheless, the results show that the matrix elements match to a satisfyingly high degree and usage of either method is sensible.

3.3.3 Speed benchmarks

Both the direct evaluation and the Moshinsky expansion methods were benchmarked for speed, so that a comparison could be made. After a dissapointing results for the Direct calculation

$\langle ij\lvert\hat{V}\rvert kl\rangle$		
Moshinsky	Direct	Δ
$-94.291\,387$	$-94.303\,113$	-1.17×10^{-2}
$-1.296\,203 \times 10^{-2}$	$-1.613\,543 \times 10^{-2}$	-3.17×10^{-3}
$-38.572\,316$	$-38.576\,820$	-4.50×10^{-3}
$-15.690\,143$	$-15.700\,959$	-1.08×10^{-2}
$-7.369\,600 \times 10^{-3}$	$-1.015\,904 \times 10^{-2}$	-2.79×10^{-3}
$0.000\,000$	$-2.227\,795 \times 10^{-3}$	-2.23×10^{-3}
$-14.120\,919$	$-14.120\,268$	6.51×10^{-4}

Table 3.2: Comparison between matrix elements in the Hartree-Fock basis calculated using the direct evaluation method and the Moshinsky expansion formula.

method, a decision was made to change the way matrix elements are calculated. While for the Moshinsky calculations the matrix elements in the harmonic oscillator basis are calculated every time they are needed, it was evident this is not optimal, as a single value could participate in forming multiple matrix elements in the Hartree-Fock basis.

N_0	$t_{\text{Hash table}}$	$t_{\text{Moshinsky}}$	$t_{\text{Hash table}}$ [min]	$t_{\text{Moshinsky}}$ [min]
6	16 min 11.323 s	28 min 49.427 s	16.19	28.82
8	25 h 18 min 54.823 s	69 h 32 min 25.250 s	1518.91	4172.42

Table 3.3: Comparison between time needed to calculate the matrix elements in the Hartree-Fock basis using both methods for two different bases.

To ensure that a matrix element in the HO basis is calculated only once – the first time it is needed, a special scheme was developed. The factorization by axial and radial part of the HO basis matrix elements was exploited, so the number of integral evaluations could be kept at minimum. Each time a matrix element is needed, a lookup is done in a hash table (see appendix A) and a value is retrieved, along with a status. If the status indicates that the matrix element is not present in the hash table, it is calculated and inserted for further availability, otherwise the recovered value is used. This process allowed for a significant increase in speed, ultimately leading to a better performance compared to the originally employed method.

For reference, using two differently sized bases the superiority of the newly developed method is clearly demonstrated. By increasing the basis, the ratio between the times required to complete increases considerably favouring the hash map method, as can be seen in table 3.3.

Chapter 4

Results & discussion

4.1 Parameters reference values

The results presented hereafter were obtained by varying the magnitudes' renomalization factor $\mathcal{V}(S,T)$ for the different channels, while using the D1M Gogny parametrization (2.41) as a reference [16].

$$V_\chi(S,T) = \mathcal{V}(S,T)V_\chi^{\mathrm{D1M}}(S,T) \tag{4.1}$$

It is inconvenient to work with the parameters W_χ, B_χ, H_χ and M_χ directly, so they could be easily converted to reference values for $V_\chi^{\mathrm{D1M}}(S,T)$ as shown in table 4.1.

$V_\chi^{\mathrm{D1M}}(S,T)$ [MeV]				
χ [fm]	$S=0,\ T=0$	$S=1,\ T=0$	$S=0,\ T=1$	$S=1,\ T=1$
0.5	−53 954.74	−1929.26	261.90	4431.82
1.0	2611.91	−279.77	−125.47	−242.87

Table 4.1: Magnutudes for the different channels and ranges in the used parametrization.

4.2 The particle-hole quasi-vacuum properties

It has been already discussed that the HTDA many-body basis is built upon a reference Slater determinant, obtained from a HF+BCS calculation. The iterative process is stopped when the change of total energy for the solution drops under 10 eV. Convergence was established in 66 iterations for this particular case with total energy of $E = -819.229\,06$ MeV.

The chemical potentials λ, the energy gaps Δ, mean-square radii $\langle\hat{r}^2\rangle$ and deformations $\langle\hat{Q}_{20}\rangle$, for neutrons and protons respectively, are given in table 4.2.

	λ [MeV]	Δ [MeV]	$\langle\hat{r}^2\rangle$ [fm^2]	$\langle\hat{Q}_{20}\rangle$ [fm^2]
Neutrons	−5.2755	0.8153	21.161	611.101
Protons	−13.2323	1.0998	19.855	383.871

Table 4.2: Characteristic quantities for protons and neutrons for $|\Phi_0\rangle$.

The mean-square radius, quadrupole and octupole moments for the mean field solution in total are as follows:

$$\langle\hat{r}^2\rangle = 20.655\,\mathrm{fm}^2$$
$$\langle\hat{Q}_{20}\rangle = 994.972\,\mathrm{fm}^2$$
$$\langle\hat{Q}_{40}\rangle = 0.4489\,\mathrm{b}^2$$

4.3 Choice of channel

The isotope ^{98}Sr was chosen deliberately, because it is far from the $N = Z$ line, so the Fermi levels for protons and neutrons are sufficiently far from one another, thus expecting little to no correlation between them. Following from that expectation, only the $T = 1$ channels were investigated and indirect inferences were made about the status of the proton-neutron interactions.

As can be seen on figure 4.1, the depopulation of the ground state, being a measure of the correlations included through HTDA, is significant for the $S = 0$, $T = 1$ channel, and conversely relatively small for the $S = 1$, $T = 1$ channel. Only at the extreme, where the Gogny interaction sees a tenfold increase, the quasi-vacuum's role retreats to around 80% and the correlations introduced in the $S = 1$, $T = 1$ channel stop being negligible. Normally it is not expected this excessively strong pairing regime to be reached and if this proves to be true, it is relatively safe to assume that the contribution of the $S = 1$, $T = 1$ channel is insignificant, therefore it is possible only its counterpart to be considered. In light of this the $S = 0$, $T = 1$ channel was expectedly chosen to be the main focus of further investigations.

4.4 Composition of the HTDA ground state

To acquire a sense of the propertries of the HTDA solution it is necessary to break down and analyse the ground state structure. In figure 4.2 a separation by weight of the single, double and triple pair excitations is given along with the reference Slater determinant contribution. It shows that the single pair transfers dominate the ground state correlations, especially until the saturation point is reached. With increase of the magnitude the triple pairs start to account for more tangible amount of correlations, but not much compared to the single and double pairs. Still they might *promote* additional double pair excitations, as observed in [5].

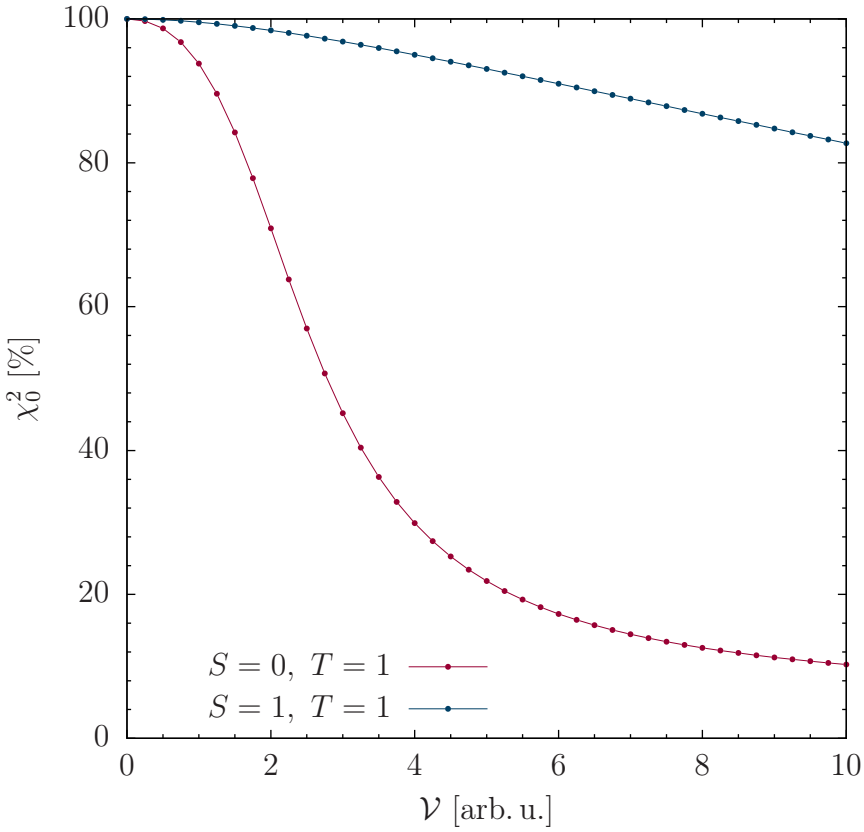

Figure 4.1: Weight of the reference Slater determinant $|\Phi_0\rangle$ in the HTDA ground state expasion for both the $T = 1$ channels, in respect to the renormalization coefficient $\mathcal{V}(S, T)$.

The dependence of pairs' populations on the pairing strength is following a pattern observed in calculations made with the delta pairing [5], thus giving a reasonable credibility to the chosen interaction.

Aditionally the constituents could be broken down by types of pairs as shown in figures 4.3a and 4.3b, where components utilizing neutron-proton pairs are not plotted as their weight do not contribute more than 1% of the total weight at any given strength, thus showing that the choice of isotope was good and the neutron-proton interplay is kept at minimum.

It is noteworthy mentioning that the amount of proton-proton pairs is significantly larger in comparison to their neutron-neutron counterparts for the single pair excitations. For two-pair transfers the one proton-proton with one neutron-neutron type of double pairs is dominant. The order by which pairs are observed might be explaned by the single-particle spectrum around the Fermi level for the reference state $|\Phi_0\rangle$, which is shown in figure E.1, appendix E.

It is evident that the single pair excitations saturate around $\mathcal{V}(S, T) = 4$ and even their weight declines slowly with increase of the magnitude. This effect is also observed in [5] and is attributed to the ratio between the interaction matrix element, which increases with the increase of $\mathcal{V}$, and excitation energy for the double pairs becoming comparable to the same ratio for single pairs'. This leads to second order corrections in perturbation theory, which drive the double

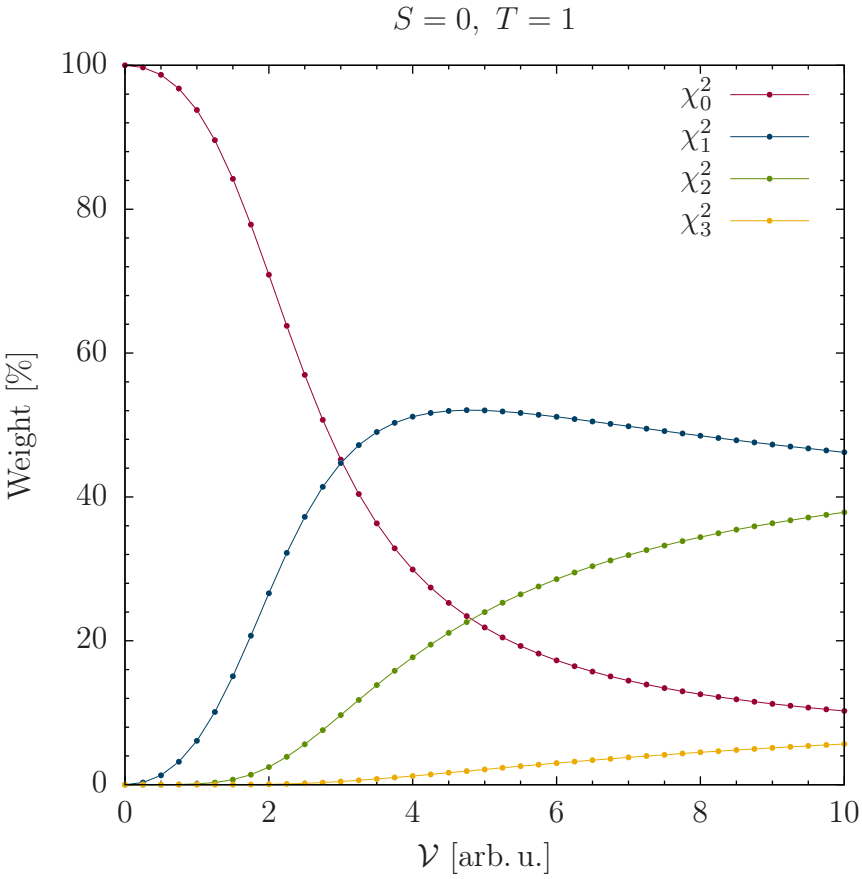

Figure 4.2: A partitioning of the different components' weights of the HTDA ground state (the particle-hole quasi-vacuum – χ_0^2, one-pair – χ_1^2, two-pair – χ_2^2 and tree-pair transfers – χ_3^2).

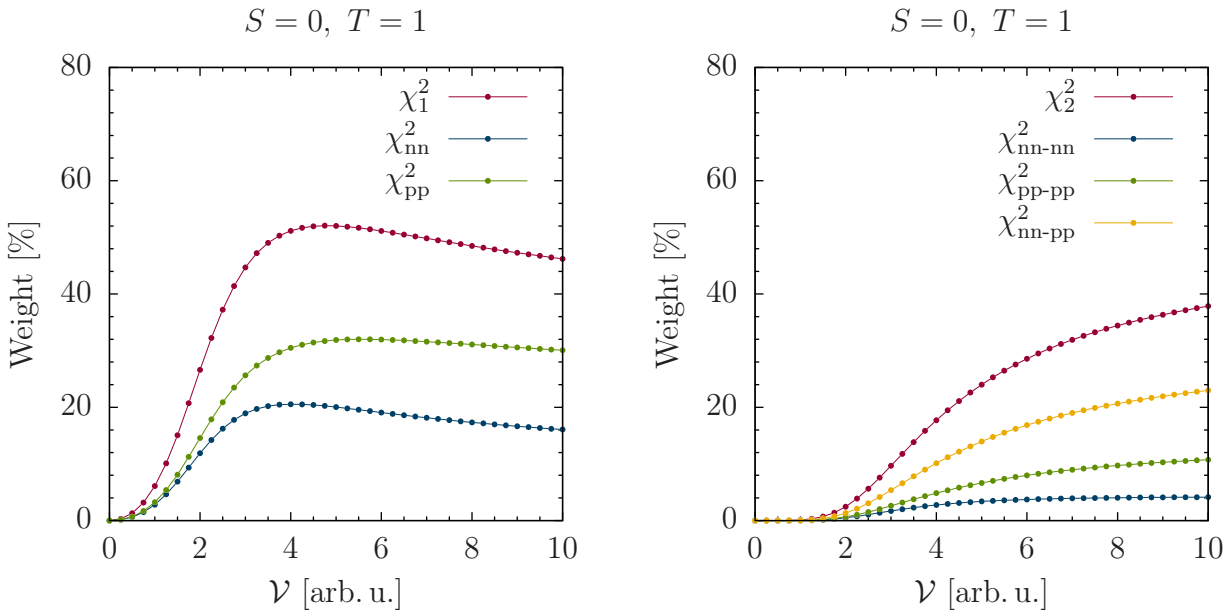

(a) Single pairs' decomposition by pair kind. *(b)* Double pairs' decomposition by pair kind.

Figure 4.3: Breakdown of the one- and two-pair transfers' types in respect to the magnitude factor.

pairs' population, reaching in magnitude the first order corrections that mainly determine the single pairs' weight, hence causing the observed effect.

4.5 The nucleus' moment of inertia

For the calculation of the moment of inertia the cranking approximation formula was used [20]:

$$I = \sum_{k,l} \frac{|\langle k|j_+|l\rangle|^2}{E_k + E_l} (u_k v_l - u_l v_k)^2 + \frac{1}{2} \sum_{k,l} \frac{|\langle k|j_+|\bar{l}\rangle|^2}{E_k + E_l} (u_k v_l - u_l v_k)^2 \tag{4.2}$$

where the first sum is over states with $\Omega_k > 0$ and the second over those with $\Omega_k = 1/2$.

A plot of the nucleus' moment of inertia is shown in figure 4.4 and it is evident that it decreases with the increase of the renormalization factor. This is not unexpected behaviour, because the amount of correlations increase with the increase of the interaction's magnitude and reduce the rigidity of the nuclear matter. While the moment of inertia apears to be quite sensitive to the change of the factor $\mathcal{V}$ for lower strengths, for the larger values it seems to saturate somewhat. Furthermore, it appears to roughly follow χ_0^2 – the ground state weight implying the two quantities are connected.

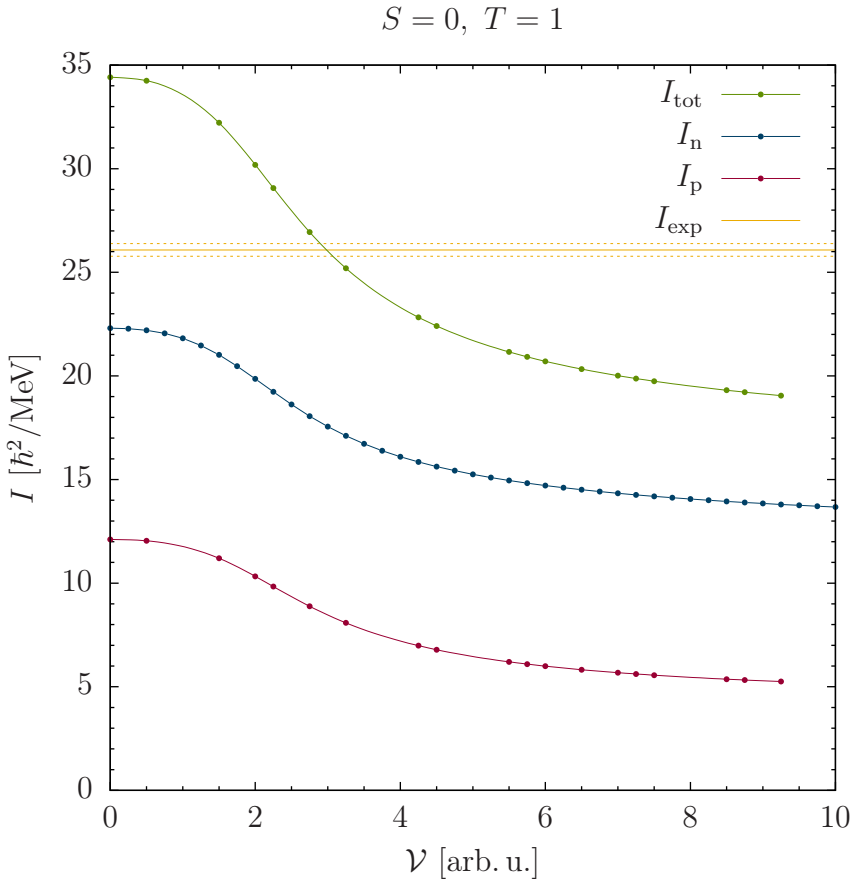

Figure 4.4: The moment of inertia for different renormalization factors and its decomposition for neutrons and protons. The experimentally obtained value is added for comparison, with dashed lines representing its standard error.

To explore this suspected connection between the total amount of correlations in the HTDA ground state and the moment of inertia their relation is presented in figure 4.5 including both

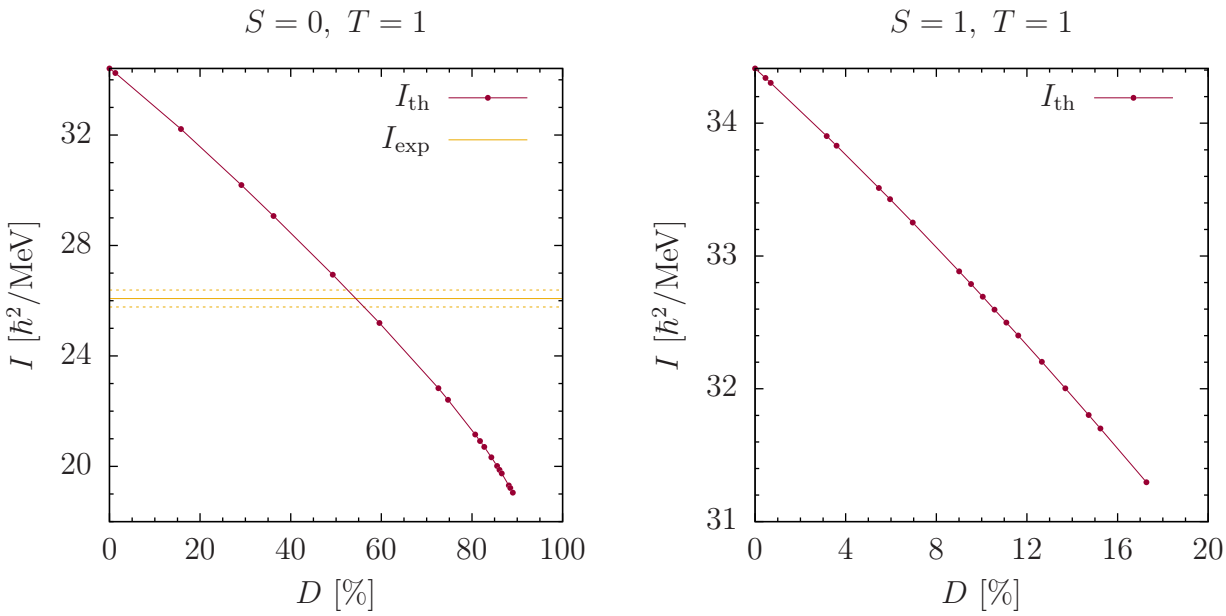

(a) The moment of inertia in respect to the ground state depopulation for the $S = 0,\ T = 1$ channel.

(b) The moment of inertia in respect to the ground state depopulation for the $S = 1,\ T = 1$ channel.

Figure 4.5: Dependence of the moment of inertia on the amount of correlations for the two $T = 1$ channels.

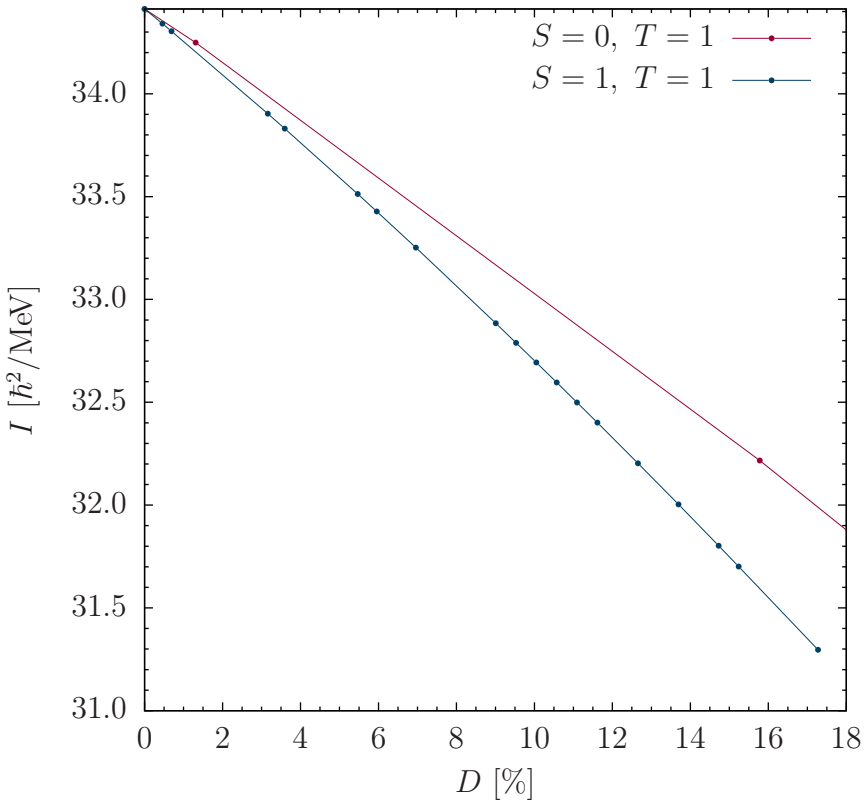

Figure 4.6: Sensitivity of the moment of inertia to correlations included through each of the two $T = 1$ channels.

the $S = 0,\ T = 1$ and $S = 1,\ T = 1$ channels. It is evident that the moment of inertia and the depopulation of the reference state correlate very well and almost linearly for both channels. It is noteworthy that both figures use a different scale, reflecting the considerably smaller amount of correlations produced by the $S = 1,\ T = 1$ channel for the same magnitudes of $\mathcal{V}$. Additionally the $S = 1,\ T = 1$ channel alone plainly is not able to generate enough correlations to reduce the moment of inertia to its experimentally obtained value (see appendix D).

To compare the moment of inertia's sensitivity to correlations induced by the two different $T = 1$ channels the available results were plotted in their common range as shown in figure 4.6. As is apparent from the slopes of the curves on the picture, even though the $S = 1$ channel produces less correlations by absolute value it does contribute more strongly to the reduction of the moment of inertia. This could be explained by inclusion of correlations beyond pairing. $S = 0,\ T = 1$ alone is able to reproduce the experimental value for the moment of inertia, but by utilising both channels simultaneously, one can expect reaching the expected value with smaller $\mathcal{V}$.

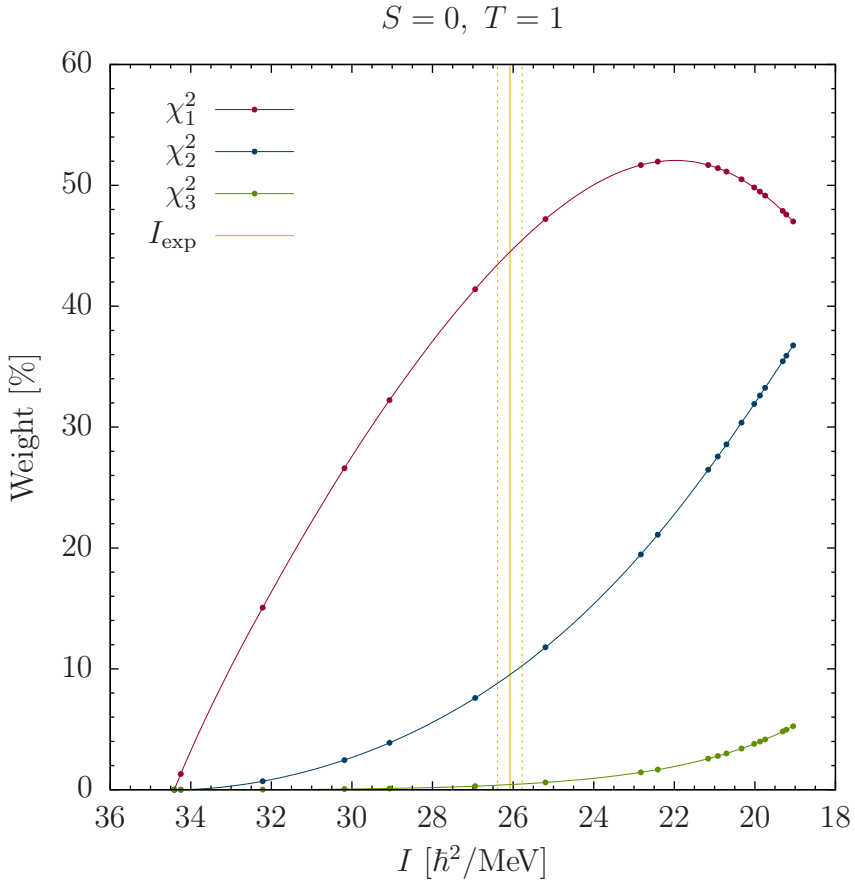

Figure 4.7: Ground state decomposition for different moments of inertia.

It is of some interest how the composition of the ground state changes between different values for, as well as how it behaves in the close proximity to a given value for the moment of inertia. The rate of change could carry significant information about the behaviour of the ground state around a value of interest, as shown in figure 4.7. For the experimental value of I, the ground

state consists predominantly of single and double pairs, while the triple pairs' contribution is negligable. From the rate of change it is discernible that in this region the moment of inertia is approximately equally sensitive to the single and double pairs' population.

Chapter 5

Outlook

The presented theoretical work treats the common problem of pairing and its role in determining the moment of inertia for an even-even nucleus. The investigation is done in the context of an explicitly particle number conserving approach - the highly truncated diagonalization approximation (HTDA), for which a finite range interaction of a gaussian type was selected as a viable candidate that should generate higher terms in the partial wave expansion. The methods and problems faced in calculating the matrix elements of the interaction are presented and emphasis is put to the consistency of the newly employed method in comparison to the already tested Moshinsky expansion procedure. The results obtained are in agreement with calculations done with a delta force and show the validity of the method selected.

The HTDA, being a purely microspcopic model, does provide a relatively good agreement with the experimental value for the moment of inertia and supplies ample information about the properties of the ground state wavefunction. It was shown that the $S = 0$, $T = 1$ channel alone accounts for the experimental value of the moment of inertia, but if both $T = 1$ channels are used it is expected the experimental value to be reached with a smaller renormalization factor. The nucleus was chosen to be neutron rich, so the neutron-proton interactions are not important and the choice was shown to be a good one, since the neutron-proton pairs of any type (single, double, triple) don't account for any tangible amount of correlations for any of the strengths explored. The moment of inertia was shown to be almost linearly dependent on the amount of correlations included through HTDA, but no discernable relation to the single, double and triple pairs' populations could be inferred.

Appendix A

The hash table data structure

A.1 General description

A *hash table* (also called *hash map*) is a data structure which maps a set of keys to a set of values. This is done by using a hash function to compute an index for an array of *buckets*, thus allowing to find the required value.

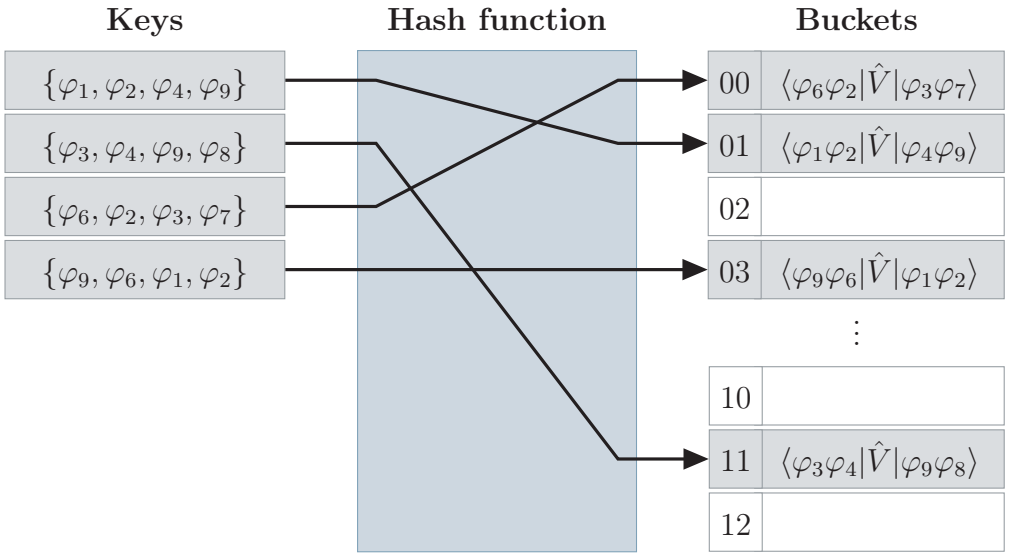

Figure A.1: Example of mapping sets of wave functions to their respective matrix elements in a hash map data structure

Ideally the hash function would be bijective, but in reality this is not the case and the mapping is most commonly surjective, meaning that actually multiple keys could be mapped onto the same value – *hash collisions*.

A hash table is on average extremely efficient for lookup-intensive applications performing as shown in table A.1. For the problem considered, an implementation from the *boost* C++ library was used by interfacing it with the existing Fortran code. This was realized by developing a

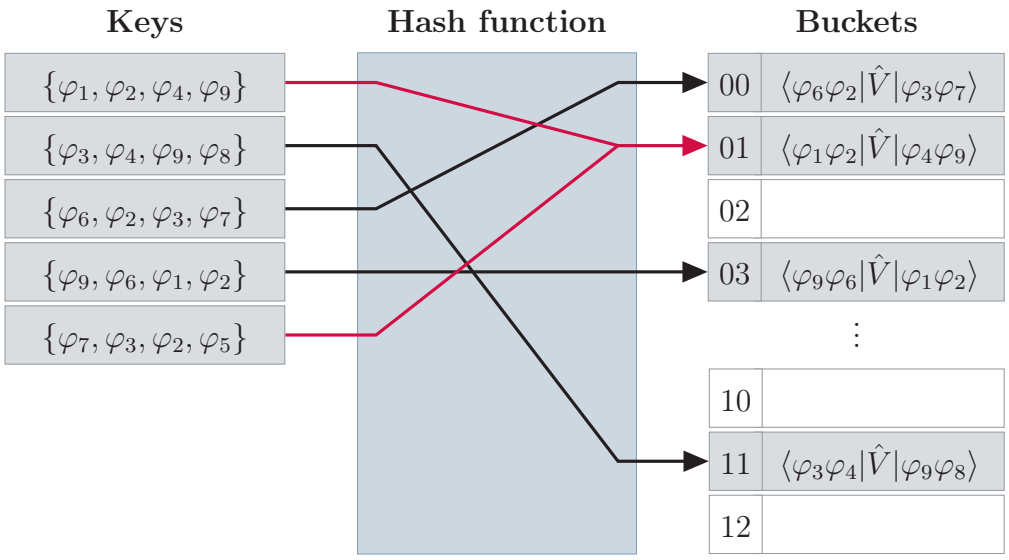

Figure A.2: Example of a hash collision

separate C++ wrapper which provides the specializations of the library templates and exposes them to the remainder of the program. Additionaly, it was assumed for simplicity that the hash function is perfect and does not generate collisions.

Although hash tables and binary search trees provide the same functionality, there are some subtle differences which make them suitable for distinctly different applications. Self-balancing binary search trees provide significantly better worst case scenarios, but they also have larger times on average (also known as *amortized times*) [21]. This would make them better suited in situations where multiple collisions are expected and have to be resolved or when ordering of the items is important. When ordering is not needed and hash collisions could be kept at minimum, hash tables provide higher efficiency. In the current work, binary trees were discarded as a viable option because of their amortized lookup and insertion times being significantly larger than those of a hash map, as can be seen in table A.1.

Time complexity (in big O notation)				
	Hash map		Self-balancing binary tree	
	Average	Worst case	Average	Worst case
Search	Amort. O(1)	O(n)	O($\log n$)	O($\log n$)
Insert	O(1)	O(n)	O($\log n$)	O($\log n$)
Delete	Amort. O(1)	O(n)	O($\log n$)	O($\log n$)

Table A.1: Comparison between self-balancing search trees and hash maps in terms of time complexities. [21]

A.2 Application

A hash map was employed to store the axial and radial parts of the gaussian matrix elements in the harmonic oscillator basis (appendix B). Only spatial parts are considered as they are

the computationally heavy elements of the evaluation. In total four tables are used – two for the short and long ranged axial part, and two for the short and long ranged radial part. Because of the factorization, the axial part of the matrix elements could be described only by four quantum numbers – $\{n_z(i), n_z(j), n_z(k), n_z(l)\}$, while the radial part is fixed by its eight quantum numbers – $\{n_r(i), n_r(j), n_r(k), n_r(l)\}$ and $\{\Lambda(i), \Lambda(j), \Lambda(k), \Lambda(l)\}$, where i, j, k, l refer to the corresponding wavefunctions [17]. As could be expected, those quantum numbers were used as keys to map the respective values obtained for the matrix elements' parts.

The hash function selected is from the family of binary polynomials – an implementation of CRC32 [22]. Although most commonly used for error detection, in this case it was preferred because of the good dispersion, support for variable length key and high speed, alongside with a simple implementaton. It proved to be adequate for the problem considered and superiror to the other algorithm examined – Fowler–Noll–Vo hashing (FNV-1a).

Appendix B

Gaussian-type interaction matrix elements

B.1 Analytical formula

It is shown in [17] that the matrix elements of the Gaussian interaction, namely the central term in the Gogny force, could be calculated by direct evaluation of two twofold integrals – one coresponding to the axial dependence and the other to the radial. The matrix element in the axially symmetric harmonic oscillator basis is given by:

$$\langle ij|\hat{V}^{(r)}|kl\rangle = N_\omega \int_0^\infty \int_0^\infty \omega_\eta \eta_1^{\Lambda_{ik}} \eta_2^{\Lambda_{jl}} e^{-\eta_1} e^{-\eta_2} d\eta_1 d\eta_2 \int_{-\infty}^\infty \int_{-\infty}^\infty \omega_\xi e^{-\xi_1^2} e^{-\xi_2^2} d\xi_1 d\xi_2 \tag{B.1}$$

N_ω is a normalization coefficient and is given by:

$$N_\omega = \frac{4}{\pi} \left\{ \frac{\left[\mu_z^2 \mu_\perp^{\sigma_\perp+4} 2^{\sigma_z} |\Lambda(i)|! \, |\Lambda(j)|! \, |\Lambda(k)|! \, |\Lambda(l)|!\right]^{-1}}{n_z(i)! n_z(j)! n_z(k)! n_z(l)! C_{n_r(i)}^{n_r(i)+|\Lambda(i)|} C_{n_r(j)}^{n_r(j)+|\Lambda(j)|} C_{n_r(k)}^{n_r(k)+|\Lambda(k)|} C_{n_r(l)}^{n_r(l)+|\Lambda(l)|}} \right\}^{\frac{1}{2}} \tag{B.2}$$

With C_k^n in (B.2) are denoted the binomial coefficients:

$$C_k^n \equiv \binom{n}{k} \tag{B.3}$$

The functions to be integrated are represented by:

$$\omega_\eta = I_\lambda \left[2 \left(1 - \frac{1}{\mu_\perp} \right) \sqrt{\eta_1 \eta_2} \right] \frac{L_i(\eta_1) L_j(\eta_2) L_k(\eta_1) L_l(\eta_2)}{\eta_1^{\overline{\Lambda}_{ik}} \eta_2^{\overline{\Lambda}_{jl}}} \tag{B.4}$$

$$\omega_\xi = H_i \left(\frac{\xi_2}{\sqrt{2}} + \frac{\xi_1}{\mu_z \sqrt{2}} \right) H_j \left(\frac{\xi_2}{\sqrt{2}} - \frac{\xi_1}{\mu_z \sqrt{2}} \right) H_k \left(\frac{\xi_2}{\sqrt{2}} + \frac{\xi_1}{\mu_z \sqrt{2}} \right) H_l \left(\frac{\xi_2}{\sqrt{2}} - \frac{\xi_1}{\mu_z \sqrt{2}} \right) \tag{B.5}$$

Where the shorthand notations are employed:

$$\mu_z = \left(1 + \frac{2\mu}{\beta_z^2}\right)^{\frac{1}{2}} \qquad \mu_\perp = 1 + \frac{\mu}{\beta_\perp^2} \tag{B.6}$$

$$\lambda = \Lambda(k) - \Lambda(i) \tag{B.7}$$

$$\sigma_\perp = |\Lambda(i)| + |\Lambda(j)| + |\Lambda(k)| + |\Lambda(l)| \tag{B.8}$$

$$\sigma_z = n_z(i) + n_z(j) + n_z(k) + n_z(l) \tag{B.9}$$

And the parameters Λ_{ij} and $\overline{\Lambda}_{ij}$ are chosen such that $\Lambda_{ij} \in \mathbb{N}$, while keeping their proper ratio:

$$\frac{\eta^{\Lambda_{ij}}}{\eta^{\overline{\Lambda}_{ij}}} \equiv \eta^{\frac{1}{2}[|\Lambda(i)|+|\Lambda(k)|]} \tag{B.10}$$

Then they have simple representations of the type:

$$\Lambda_{ij} = \left\lceil \frac{1}{2}\left[|\Lambda(i)| + |\Lambda(j)|\right] \right\rceil \tag{B.11}$$

$$\overline{\Lambda}_{ij} = \Lambda_{ij} - \frac{1}{2}\left[|\Lambda(i)| + |\Lambda(j)|\right] \tag{B.12}$$

B.2 Numerical evaluation

A set of functions in Fortran were developed to facilitate the numerical evaluation of both the axial and radial integrals. Not only the nodes at which functional values are required were calculated, but the quadrature weights as well, up to a configured arbitrary order. Compensated summations (namely the Kahan summation algorithm) are used throughout the code to ensure that the numerical errors are kept minimal [23].

B.2.1 Axial part

For the axial integral a Gauss-Hermite quadrature was used [24]:

$$\int_{-\infty}^{+\infty}\int_{-\infty}^{+\infty} \omega_\xi(\xi_1, \xi_2) e^{-\xi_1^2} e^{-\xi_2^2} d\xi_1 d\xi_2 \approx \sum_{i=1}^{m}\sum_{j=1}^{n} w_i(m) w_j(n) \omega_\xi(\xi_i^{(1)}, \xi_j^{(2)}) \tag{B.13}$$

where $\xi_i^{(1)}$ is i-th root of the Hermite polynomial $H_m(x)$, $\xi_j^{(2)}$ is j-th root of the Hermite polynomial $H_n(x)$ and $w_i(m)$, $w_j(n)$ are the weights respectively:

$$w_i(n) = \frac{2^{n-1} n! \sqrt{\pi}}{n^2 [H_{n-1}(x_i)]^2} \quad \text{where} \quad H_n(x_i) = 0 \tag{B.14}$$

The order of the quadrature rule is automatically adjusted depending on the Hermite polynomials' order in ω_ξ, so that the integration is analytically exact.

The roots and weights were checked against Maple and a standard set of mathematical tables [24]. The values match to a scale of 10^{-12} accross the tested orders range, which spanned from 0 to 10.

B.2.2 Radial part

For the radial part a generalized Gauss-Laguerre quadrature was used [25, 26]:

$$\int_0^\infty \int_0^\infty \omega_\eta(\eta_1, \eta_2) \eta_1^{\Lambda_{ik}} \eta_2^{\Lambda_{jl}} e^{-\eta_1} e^{-\eta_2} d\eta_1 d\eta_2 \approx \sum_{p=1}^{m} \sum_{q=1}^{n} w_i(p, \Lambda_{ik}) w_j(q, \Lambda_{jl}) \omega_\eta(\eta_i^{(1)}, \eta_j^{(2)}) \tag{B.15}$$

where $\eta_i^{(1)}$ is i-th root of the associated Laguerre polynomial $L_m^{\Lambda_{ik}}(x)$, $\eta_j^{(2)}$ is j-th root of the associated Laguerre polynomial $L_n^{\Lambda_{jl}}(x)$ and $w_i(m, \Lambda_{ik})$, $w_j(n, \Lambda_{jl})$ are the weights respectively:

$$w_i(n, \Lambda) = \frac{\binom{n+\Lambda}{\Lambda} \Lambda!}{(n+1)^2} \frac{x_i}{\left[L_{n+1}^{\Lambda}(x_i)\right]^2} \quad \text{where} \quad L_n^{\Lambda}(x_i) = 0 \tag{B.16}$$

Because the function ω_η cannot be represented by a polynomial, in contrast to ω_ξ, in this case the integration is analytically, as well as numerically approximate. For practical reasons and because the modified Bessel function contained in ω_η introduces somewhat unwanted behaviour, large order quadrature rules are used ($n > 30$) to keep accuracy at a satisfactory level.

An extensive accuracy benchmark for the weights and roots was done using both Maple and mathematical tables [25,26]. Even though deviations from the expected value were several hundred to thousand times larger than those observed for the axial integrals, they were consistently below 10^{-8}, even for the highest of the tested orders. This provided enough confidence in the numerical results obtained with the method.

Appendix C

The Gogny force matrix element

C.1 In the harmonic oscillator basis

Using the given parametrisation of the cenral term of the Gogny force:

$$\begin{aligned}\hat{V}_{\text{Gogny}} &= \sum_{S,T,\chi} \left[W_\chi + (-1)^{S+1} B_\chi - (-1)^{T+1} H_\chi - (-1)^{S+T} M_\chi\right] \hat{\mathbb{P}}^S \hat{\mathbb{P}}^T \hat{V}^{(r,\sigma,\tau)} \\ &= \sum_{S,T,\chi} V_\chi(S,T) \hat{\mathbb{P}}^S \hat{\mathbb{P}}^T \hat{V}^{(r,\sigma,\tau)}\end{aligned} \tag{C.1}$$

Where the projection operators are given through the spin and isospin exchange operators by the equations:

$$\hat{\mathbb{P}}^S = \frac{1}{2}\left[1 - (-1)^S \hat{P}_\sigma\right] \qquad \hat{\mathbb{P}}^T = \frac{1}{2}\left[1 - (-1)^T \hat{P}_\tau\right] \tag{C.2}$$

The spatial, spin and isospin components are separable in the potential $\hat{V}^{(r,\sigma,\tau)}$:

$$\hat{V}^{(r,\sigma,\tau)} = \hat{V}^{(r)} \hat{V}^{(\sigma)} \hat{V}^{(\tau)} \tag{C.3}$$

and additionally they commute freely with one another:

$$\left[\hat{V}^{(r)}, \hat{V}^{(\sigma)}\right] = 0 \tag{C.4}$$

$$\left[\hat{V}^{(r)}, \hat{V}^{(\tau)}\right] = 0 \tag{C.5}$$

$$\left[\hat{V}^{(\sigma)}, \hat{V}^{(\tau)}\right] = 0 \tag{C.6}$$

Having in mind that:

$$\langle ij|\hat{V}^{(\sigma)}|kl\rangle = \delta_{\sigma_i\sigma_k}\delta_{\sigma_j\sigma_l} \tag{C.7}$$

$$\langle ij|\hat{V}^{(\tau)}|kl\rangle = \delta_{\tau_i\tau_k}\delta_{\tau_j\tau_l} \tag{C.8}$$

it is easy to calculate the projected spin and isospin parts:

$$\begin{aligned} G(S) =&\langle ij|\hat{\mathbb{P}}^S\hat{V}^{(\sigma)}|kl\rangle = \frac{1}{2}\langle ij|\left[1-(-1)^S\hat{P}_\sigma\right]\hat{V}^{(\sigma)}|kl\rangle \\ =&\frac{1}{2}\left[\delta_{\sigma_i\sigma_k}\delta_{\sigma_j\sigma_l}+(-1)^{S+1}\delta_{\sigma_i\sigma_l}\delta_{\sigma_j\sigma_k}\right] \end{aligned} \tag{C.9}$$

$$\begin{aligned} G(\mathrm{T}) =&\langle ij|\hat{\mathbb{P}}^{\mathrm{T}}\hat{V}^{(\tau)}|kl\rangle = \frac{1}{2}\langle ij|\left[1-(-1)^T\hat{P}_\tau\right]\hat{V}^{(\tau)}|kl\rangle \\ =&\frac{1}{2}\left[\delta_{\tau_i\tau_k}\delta_{\tau_j\tau_l}+(-1)^{T+1}\delta_{\tau_i\tau_l}\delta_{\tau_j\tau_k}\right] \end{aligned} \tag{C.10}$$

or rewriting to obtain a single spin-isospin projection:

$$\begin{aligned} G(S,T) =&\langle ij|\hat{\mathbb{P}}^S\hat{\mathbb{P}}^{\mathrm{T}}\hat{V}^{(\sigma)}\hat{V}^{(\tau)}|kl\rangle = \underbrace{\langle ij|\hat{\mathbb{P}}^S\hat{V}^{(\sigma)}|kl\rangle}_{G(S)}\underbrace{\langle ij|\hat{\mathbb{P}}^T\hat{V}^{(\tau)}|kl\rangle}_{G(T)} = \\ =&G(S)G(T) = \frac{1}{4}\left[\delta_{\sigma_i\sigma_k}\delta_{\sigma_j\sigma_l}+(-1)^{S+1}\delta_{\sigma_i\sigma_l}\delta_{\sigma_j\sigma_k}\right]\left[\delta_{\tau_i\tau_k}\delta_{\tau_j\tau_l}+(-1)^{T+1}\delta_{\tau_i\tau_l}\delta_{\tau_j\tau_k}\right] \end{aligned} \tag{C.11}$$

The matrix elements are obtained straightforwardly from (C.1) by applying the projection operators, thus separating the spin-isospin part and then substituting from (C.11):

$$\begin{aligned} \langle ij|\hat{V}_{\mathrm{Gogny}}|kl\rangle =&\sum_{S,T,\chi}V_\chi(S,T)\langle ij|\hat{\mathbb{P}}^S\hat{\mathbb{P}}^{\mathrm{T}}\underbrace{\hat{V}^{(\sigma)}\hat{V}^{(\tau)}\hat{V}^{(r)}}_{\hat{V}^{(r,\sigma,\tau)}}|kl\rangle \\ =&\langle ij|\hat{V}^{(r)}|kl\rangle\sum_{S,T,\chi}V_\chi(S,T)G(S,T) \end{aligned} \tag{C.12}$$

The possible problems connected to and numerical methods used for calculating the spatial part of the matrix element – $\langle ij|\hat{V}^{(r)}|kl\rangle$ are thoroughly considered in appendix B.

C.2 In the Hartree-Fock basis

The matrix element in the Hartree-Fock basis is simply calculated by using the known expansion coefficients c_{ij}:

$$\langle ij|\hat{V}|kl\rangle\Big|_{\mathrm{HF}} = \sum_{S,T,\chi}\sum_{n,o,p,q}c_{in}c_{jo}c_{kp}c_{lq}V_\chi(S,T)G(S,T)\langle no|\hat{V}^{(r)}|pq\rangle\Big|_{\mathrm{HO}} \tag{C.13}$$

and is then antisymmetrized:

$$\langle ij|\hat{V}|\widetilde{kl}\rangle = \langle ij|\hat{V}|kl\rangle - \langle ij|\hat{V}|lk\rangle \tag{C.14}$$

Appendix D

The ^{98}Sr moment of inertia's experimental value

To obtain the moment of inertia's experimental value, the well known semiclassical formula is used [11]:

$$E(J) - E(0) = \frac{1}{2I} J(J+1) \tag{D.1}$$

By plotting the dependence and performing a linear fit, the slope is determined (figure D.1), from which the moment of inertia is straightforwardly calculated.

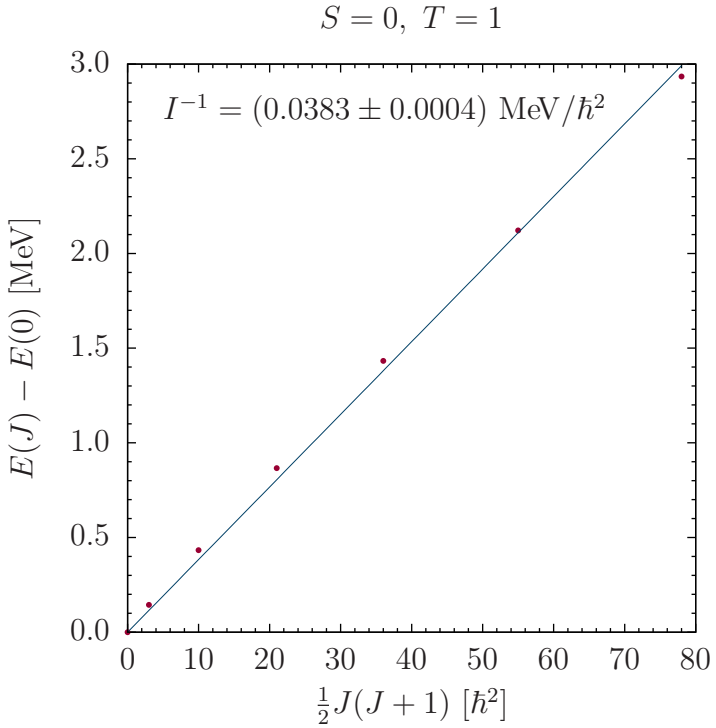

Figure D.1: Change of the rotational band energy with increase of the total angular momentum. Data was taken from the ENSDF database [27].

Appendix E

Single particle spectra

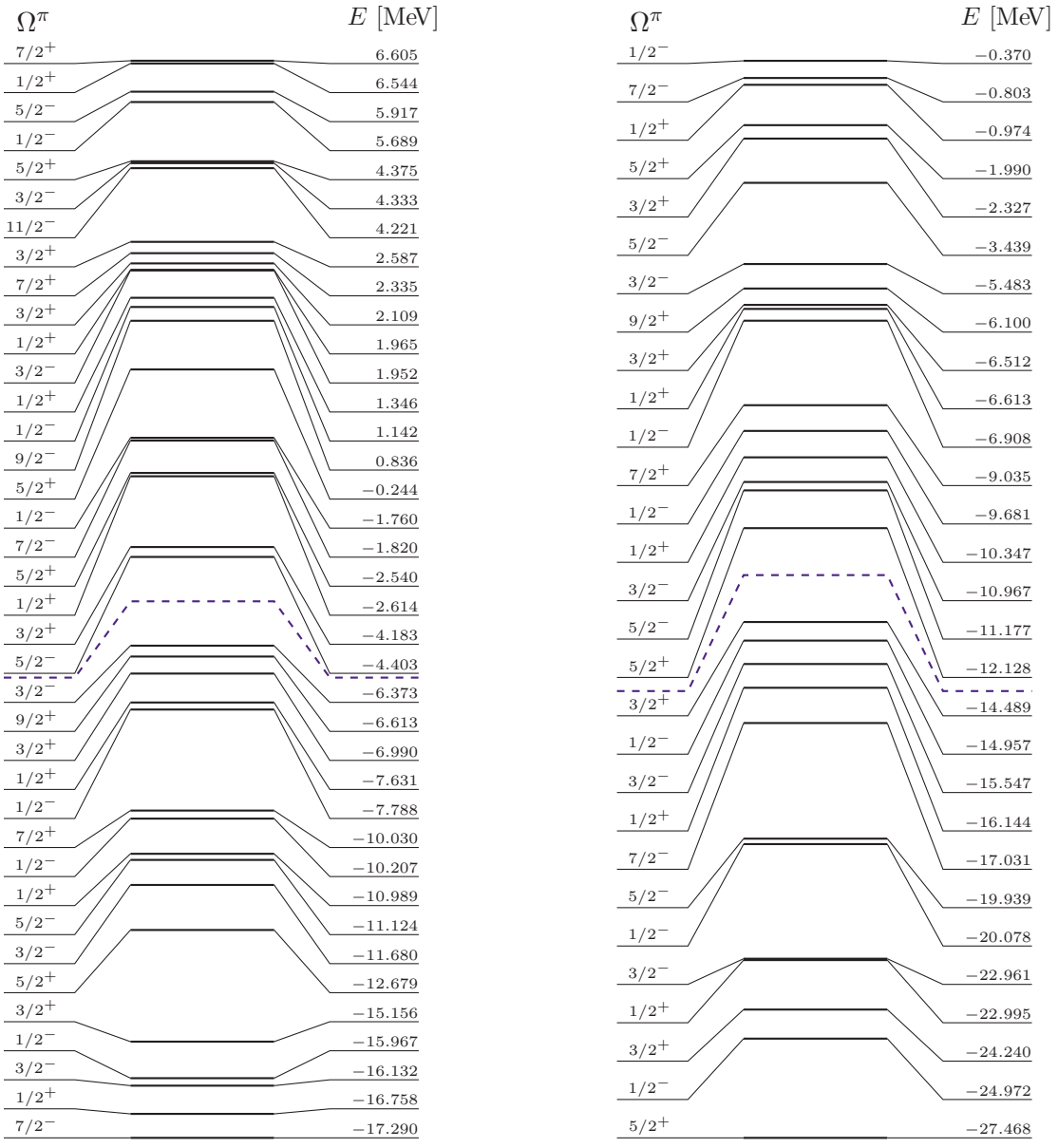

(a) Neutrons single particle spectrum. *(b)* Protons single particle spectrum.

Figure E.1: Single particle spectra (the purple dashed line is the fermi level).

Bibliography

[1] K. Sieja et al. *Particle number conserving approach to correlations*, Int. J. Mod. Phys. E **16**, 289-297 (2007), http://dx.doi.org/10.1142/S0218301307005727

[2] L. Bonneau, P. Quentin, K. Sieja *Ground-state properties of even-even $N = Z$ nuclei within the Hartree-Fock-BCS and higher Tamm-Dancoff approaches*, Phys. Rev. C **76**, 014304 (2007), http://dx.doi.org/10.1103/PhysRevC.76.014304

[3] N. Pillet, P. Quentin, J. Libert *Pairing correlations in an explicitly particle-number conserving approach*, Nucl. Phys. A **697**, 141-163 (2002), http://dx.doi.org/10.1016/S0375-9474(01)01240-4

[4] H. Naïdja et al. *Pairing and vibrational correlations in the higher Tamm-Dancoff approximation (HTDA) approach*, Phys. Rev. C **81**, 044320 (2010), http://dx.doi.org/10.1103/PhysRevC.81.044320

[5] J. Le Bloas et al. *Effect of pairing correlations on the isospin-mixing parameter in deformed $N = Z$ even-even nuclei*, Phys. Rev. C **86**, 034332 (2012), http://dx.doi.org/10.1103/PhysRevC.86.034332

[6] J. Le Bloas *Mélange d'isospin et désintégration β*, PhD thesis (unpublished), University Bordeaux 1 (2011)

[7] H. Laftchiev et al. *A particle-number conserving description of rotational correlated states*, Nucl. Phys. A **845**, 33–57 (2010), http://dx.doi.org/10.1016/j.nuclphysa.2010.04.014

[8] W. Greiner, J. A. Maruhn *Nuclear Models* (1997), Springer-Verlag, ISBN 9783540780465

[9] Duy Duc Dao *Corrélations d'appariement dans les noyaux atomiques avec une interaction résiduelle de portée finie*, Internship report (unpublished), University Bordeaux 1 (2012)

[10] F. Chappert, M. Girod, S. Hilaire *Towards a new Gogny force parameterization: Impact of the neutron matter equation of state*, Phys. Lett. B **668**, 420-424 (2008), http://dx.doi.org/10.1016/j.physletb.2008.09.017

[11] P. Ring, P. Schuck *The Nuclear Many-Body Problem* (2004), Springer, ISBN 9783540212065

[12] R. Woods, D. Saxon *Diffuse surface optical model for nucleon-nuclei scattering*, Phys. Rev. **95**, 577–578 (1954), http://dx.doi.org/10.1103/PhysRev.95.577

[13] R. Casten *Nuclear Structure from a Simple Perspective* (2000), Oxford University Press, ISBN 9780198507246

[14] L. Bonneau et al. *Effects of core polarization and pairing correlations on ground-state properties of odd-mass nuclei*, Int. J. Mod. Phys. E **20**, 252-258 (2011), http://dx.doi.org/10.1142/S0218301311017594

[15] G. Wick *The Evaluation of the Collision Matrix*, Phys. Rev. **80**, 268–272 (1950), http://dx.doi.org/10.1103/PhysRev.80.268

[16] S. Goriely et al. *First Gogny-Hartree-Fock-Bogoliubov Nuclear Mass Model*, Phys. Rev. Lett. **102**, 242501 (2009), http://dx.doi.org/10.1103/PhysRevLett.102.242501

[17] К. Шегунов *Пресмятане на матрични елементи за взаимодействие на Gogny при разширено Тамм–Данков приближение*, Bachelor's thesis (unpublished), Faculty of physics, Sofia university "St. Kliment Ohridski" (2011)

[18] M. Beiner et al. *Nuclear ground-state properties and self-consistent calculations with the skyrme interaction: (I). Spherical description*, Nucl. Phys. A **238**, 29-69 (1975), http://dx.doi.org/10.1016/0375-9474(75)90338-3

[19] P. Quentin *Skyrme's interaction in the asymptotic basis*, J. Phys. France **33(5-6)**, 457-463 (1972), http://dx.doi.org/10.1051/jphys:01972003305-6045700

[20] D. W. L. Sprung et al. *Collective gyromagnetic ratio and moment of inertia from density-dependent Hartree-Fock calculations*, Nucl. Phys. A **326**, 37-46 (1979), http://dx.doi.org/10.1016/0375-9474(79)90364-6

[21] D. E. Knuth *The art of computer programming* vol. 3 (1997), Addison-Wesley, ISBN 9780201896831

[22] K. Brayer, J. L. Hammond Jr. *Evaluation of error detection polynomial performance on the AUTOVON channel* (1975), IEEE National Telecommunications Conference, pp. 8-25

[23] W. Kahan *Pracniques: further remarks on reducing truncation errors*, Commun. ACM **8**, 40 (1965), http://dx.doi.org/10.1145/363707.363723

[24] M. Abramowitz, I. A. Stegun *Handbook of Mathematical Functions: With Formulas, Graphs, and Mathematical Tables* (1972), Dover Publ., ISBN 9780486612720

[25] P. Concus et al. *Tables for the evaluation of* $\int_0^\infty x^\beta e^{-x} f(x)dx$ *by Gauss-Laguerre quadrature*, Math. Comp. **17**, 245-256 (1963), http://dx.doi.org/10.1090/S0025-5718-1963-0158534-9

[26] P. Rabinowitz, G. Weiss *Tables of abcissas and weights for numerical evaluation of integrals of the form* $\int_0^\infty e^{-x}x^n f(x)dx$, Math. Comp. **14**, 285-294 (1959), http://dx.doi.org/10.1090/S0025-5718-1959-0107992-3

[27] Lawrence Berkeley National Laboratory *Evaluated Nuclear Structure Data File (ENSDF) database*, http://www.nndc.bnl.gov/ensdf/